Interactions of the Novel Antimicrobial Peptide Buforin 2 with Lipid Bilayers: Proline as a Translocation Promoting Factor†

Satoe Kobayashi,‡ Kenta Takeshima,§ Chan Bae Park,|| Sun Chang Kim,|| and Katsumi Matsuzaki*,§

Graduate Schools of Pharmaceutical Sciences and Biostudies, Kyoto University, Kyoto 606-8501, Japan, and Department of Biological Sciences, Korea Advanced Institute of Science and Technology, Taejon 305-701, Korea

Received February 29, 2000; Revised Manuscript Received May 8, 2000

ABSTRACT: Buforin 2 is an antimicrobial peptide discovered in the stomach tissue of the Asian toad *Bufo bufo gargarizans*. The 21-residue peptide with +6 net charge shows antimicrobial activity an order of magnitude higher than that of magainin 2, a membrane-permeabilizing antimicrobial peptide from *Xenopus laevis* [Park, C. B., Kim, M. S., and Kim, S. C. (1996) *Biochem. Biophys. Res. Commun. 218*, 408−413]. In this study, we investigated the interactions of buforin 2 with phospholipid bilayers in comparison with magainin 2 to obtain insight into the mechanism of action of buforin 2. Equipotent Trp-substituted peptides were used to fluorometrically monitor peptide−lipid interactions. Circular dichroism measurements showed that buforin 2 selectively bound to liposomes composed of acidic phospholipids, assuming a secondary structure similar to that in trifluoroethanol/water, which is an amphipathic helix distorted around Pro^{11} with a flexible N-terminal region [Yi, G. S., Park, C. B., Kim, S. C., and Cheong, C. (1996) *FEBS Lett. 398*, 87−90]. Magainin 2 induced the leakage of a fluorescent dye entrapped within lipid vesicles coupled to lipid flip-flop. These results have been interpreted as the formation of a peptide−lipid supramolecular complex pore [Matsuzaki, K. (1998) *Biochim. Biophys. Acta 1376*, 391−400]. Buforin 2 exhibited much weaker membrane permeabilization activity despite its higher antimicrobial activity. In contrast, buforin 2 was more efficiently translocated across lipid bilayers than magainin 2. These results suggested that the ultimate target of buforin 2 is not the membrane but intracellular components. Furthermore, buforin 2 induced no lipid flip-flop, indicating that the mechanism of translocation of buforin 2 is different from that of magainin 2. The role of Pro was investigated by use of a P11A derivative of buforin 2. The derivation caused a change to magainin 2-like secondary structure and membrane behavior. Pro^{11} was found to be a very important structural factor for the unique properties of buforin 2.

Recently, a number of antimicrobial peptides composed of 15−40 amino acids have been discovered in various organisms (*1*). These peptides play significant roles in host defense against invading pathogenic microorganisms. Many of these peptides are considered to act on the lipid matrix of bacterial cell membranes, destroying the barrier property and killing the bacteria, although the actual mechanisms of action are still under argument. For magainin 2, a representative antimicrobial peptide discovered in the skin of the African clawed frog *Xenopus laevis* (*2*−*4*), we have proposed the following model. The peptide forms an amphipathic helix in lipid bilayers, which essentially lies parallel to the membrane surface (*5*). Five helices on average together with several surrounding lipids form a membrane-spanning pore comprising a dynamic, peptide−lipid supramolecular complex, which allows not only ion transport but also rapid flip-flop of membrane lipids (*6*). Upon disintegration of the pore, a fraction of the peptide molecules is stochastically translocated into the inner leaflet (*7, 8*). These processes can be controlled by modifying the peptide charge (*9*). This mechanism is universally applicable to other amphiphathic peptides such as mastoparan X (*10*) and PGLa (*11*).

In 1996, the antimicrobial peptide buforin 1 was isolated from the stomach tissue of the Asian toad *Bufo bufo gargarizans*, and a more potent peptide, buforin 2, was derived from buforin 1 (*12*). Buforins show much stronger antimicrobial activities against a broad spectrum of microorganisms compared with magainin 2. Interestingly, the mechanism of action of buforin 2 has been suggested to be different from those of membrane-acting peptides, although the physicochemical properties of the peptide are similar to those of other peptides in terms of amphipathicity and basicity (Table 1). Park et al. (*13*) reported that buforin 2 kills bacteria without cell lysis and has strong affinity for DNA and RNA, suggesting that the target of buforin 2 is not the cell membrane but intracellular nucleic acids. Indeed, buforin 1 was reported to show sequence homology with the N-terminus of histone H2A (*14*). Several peptides are also considered to have mechanisms of action other than membrane permeabilization (*15*−*18*). Even for these peptides, peptide−membrane interactions are important because

† Supported in part by the Mochida Memorial Foundation for Medical and Pharmaceutical Research, the Kato Memorial Bioscience Foundation, the Mitsubishi Foundation, and Novartis Foundation (Japan) for the Promotion of Science.

* To whom correspondence should be addressed: Telephone 81-75-753-4574; fax 81-75-761-2698; e-mail katsumim@pharm.kyoto-u.ac.jp.

‡ Graduate School of Pharmaceutical Sciences, Kyoto University.

§ Graduate School of Biostudies, Kyoto University.

|| Korea Advanced Institute of Science and Technology.

10.1021/bi0004549 CCC: $19.00
Published on Web 06/30/2000

Table 1: Properties of the Peptides Used

peptide	sequence	charge[a]	*H* (kcal/mol)[b]
MG2	GIGKWLHSAKKFGKAFVGEIMNS	+3	−0.393
BF2	TRSSRAGLQWPVGRVHRLLRK	+6	−0.232
P11A-BF2	TRSSRAGLQWAVGRVHRLLRK	+6	−0.212

[a] Approximate charges at physiological pH. The α-NH_2 and His group were assumed to be completely protonated and deprotonated, respectively. [b] Mean residue hydrophobicity, *H*, was calculated from the hydrophobicities of individual amino acid side chains, estimated from the partition coefficients of *N*-acetyl amino acid amides between water and *n*-octanol (*39*).

the peptides should first bind to and then cross the cell membranes before entering cells.

In this study, the interactions of buforin 2 with phospholipid membranes were investigated in detail by use of liposomes as a model membrane system, and the results were compared with those of magainin 2. Buforin 2 was found to be translocated across the membranes efficiently without inducing significant membrane permeabilization or lipid flip-flop. Furthermore, the Pro^{11} residue appears to be a key structural factor for this unique property of buforin 2.

MATERIALS AND METHODS

Materials. F10W-buforin 2 (BF2),[1] F5W-magainin 2 (MG2), and P11A,F10W-buforin 2 (P11A-BF2) were synthesized by the standard Fmoc-based solid-phase method, as previously described (*5*). The purity of the synthesized peptides was determined by analytical HPLC and ion-spray mass spectroscopy. DNS-PE, C_6-NBD-PC, and C_{12}-NBD-PA were purchased from Avanti Polar Lipids (Alabaster, AL). EYPG, EYPC, EYPE, valinomycin, and trypsin−chymotrypsin inhibitor were obtained from Sigma (St. Louis, MO). Trypsin was purchased from Wako (Tokyo, Japan). ANTS, DPX, and $DiSC_2(5)$ were obtained from Molecular Probes (Eugene, OR). Spectrograde organic solvents were supplied by Dojindo (Kumamoto, Japan). All other chemicals from Wako were of special grade. A HEPES−NaOH buffer (10 mM HEPES/45 mM NaCl/1 mM EDTA, pH 7.4) was prepared with double-distilled water. For CD measurements, phosphate buffer (10 mM sodium phosphate/45 mM NaCl/1 mM EDTA, pH 7.4) was used. Phosphate-buffered saline, pH 7.4, was purchased from Sigma for hemolysis measurements.

Vesicle Preparation. LUVs were prepared and characterized as described elsewhere (*6*). Briefly, a lipid film, after drying under vacuum overnight, was hydrated with the buffer (for ANTS/DPX leakage measurements, 6 mM ANTS/24 mM DPX in HEPES−NaOH buffer) and vortex-mixed to produce MLVs. The suspension was subjected to five cycles of freezing and thawing (for ANTS/DPX encapsulated LUVs, 10 cycles because of high lipid concentrations), and then extruded through polycarbonate filters (100 nm pore size filter, 21 times). SUVs for CD measurements were produced by sonication of freeze−thawed MLVs in ice−water under a nitrogen atmosphere. The lipid concentration was determined in triplicate by phosphorus analysis (*19*).

CD Spectra. CD spectra were measured on a Jasco J-720 apparatus interfaced to an NEC PC-9801 microcomputer, using a 1-mm path-length quartz cell to minimize the absorbance due to buffer components. The instrumental outputs were calibrated with nonhygroscopic ammonium *d*-camphor-10-sulfonate (*20*). Eight scans were averaged for each sample and the averaged blank spectra (vesicle suspension) were subtracted. The peptide concentration was 25 μM. The absence of any optical artifacts was confirmed as described elsewhere (*21*).

ANTS/DPX Leakage. Immediately after the extrusion, vesicles containing ANTS/DPX were separated from free ANTS and DPX on a Bio-Gel A-1.5m column. The release of ANTS and/or DPX from the LUVs was fluorometrically monitored on a Shimadzu RF-5000 spectrofluorometer at an excitation wavelength of 353 nm and an emission wavelength of 520 nm. The maximum fluorescence intensity corresponding to 100% leakage was determined by the addition of 10% (w/v) Triton X-100 (20 μL) to 2 mL of the sample. The apparent percent leakage value was calculated according to

$$\%\ \text{apparent leakage} = 100(F - F_0)/(F_t - F_0) \quad (1)$$

F and F_t denote fluorescence intensities before and after detergent addition, respectively. F_0 represents fluorescence of intact vesicles. Ladokhin et al. (*22*) described the details of the ANTS/DPX leakage experiments.

Diffusion Potential Assay. The leakage of small ions from LUVs induced by peptides was assessed by the diffusion potential assay (*23, 24*). The fluorescent, potential-sensitive dye $DiSC_2(5)$ in MeOH (7 μL) was diluted into 1941 μL of Na^+-containing buffer (15 mM Na_2SO_4/10 mM HEPES−NaOH/1 mM EDTA, pH 7.4), and an aliquot (14 μL) of liposome suspension in K^+-containing buffer (15 mM K_2SO_4/10 mM HEPES−NaOH/1 mM EDTA, pH 7.4) was then added. The final phospholipid concentration was 215 μM. The mixture was stirred for 5 min and valinomycin (8 μL, 2.5 μM in EtOH) was added to the suspension to slowly create an inside-negative diffusion potential, which led to quenching of dye fluorescence. After fluorescence had been stabilized for 2−3 min, 30 μL of a peptide solution in buffer (10 mM HEPES−NaOH/1mM EDTA, pH 7.4) was added to bring the total sample volume to 2 mL. The subsequent

[1] Abbreviations: ANTS, 8-aminonaphthalene-1,3,6-trisulfonic acid, disodium salt; BF2, F10W-buforin 2; CD, circular dichroism; C_6-NBD-PC, 1-palmitoyl-2-[6-[(7-nitrobenz-2-oxa-1,3-diazol-4-yl)amino]caproyl]-L-α-phosphatidylcholine; C_{12}-NBD-PA, 1-oleoyl-2-[12-[(7-nitrobenz-2-oxa-1,3-diazol-4-yl)amino]dodecanoyl]-L-α-phosphatidic acid (sodium salt); $DiSC_2(5)$, 3,3′-diethylthiadicarbocyanine iodide; DNS-PE, *N*-[[(5-(dimethylamino)naphthyl]-1-sulfonyl]-L-α-phosphatidylethanolamine (derived from egg yolk); DPoPE, dipalmitoleoyl-L-α-phosphatidylethanolamine; DPX, *p*-xylenebispyridinium bromide; EYPC, egg yolk L-α-phosphatidylcholine; EYPE, egg yolk L-α-phosphatidylethanolamine; EYPG, L-α-phosphatidyl-DL-glycerol enzymatically converted from egg yolk L-α-phosphatidylcholine; Fmoc, fluoren-9-ylmethoxycarbonyl; HPLC, high-performance liquid chromatography; L/P, lipid to peptide molar ratio; LUVs, large unilamellar vesicles; MG2, F5W-magainin 2; MIC, minimal inhibitory concentration; MLVs, multilamellar vesicles; P11A-BF2, P11A,F10W-buforin 2; PC, phosphatidylcholine; PG, phosphatidylglycerol; RET, resonance energy transfer; SUVs, small unilamellar vesicles; TFE, 2,2,2-trifluoroethanol; T_H, lamellar to hexagonal II phase transition temperature; TSB, trypticase soy broth.

dissipation of diffusion potential, as reflected by an increase in fluorescence, was monitored by spectrofluorometry with excitation and emission wavelengths of 620 and 670 nm, respectively.

Translocation. Lipid film (EYPC/EYPG/DNS-PE = 50/45/5) was hydrated with 200 μM trypsin solution in buffer, and LUVs were prepared. Trypsin−chymotrypsin inhibitor (2000 μM) was added to the same volume of LUV suspension to inactivate the enzyme outside the vesicles. Peptides ([peptide] = 1 μM) were added to the membranes ([lipid] = 215 μM). Sensitized dansyl fluorescence at 510 nm was recorded on excitation of the Trp residues at 280 nm. A decrease in fluorescence implied digestion of the fluorescent peptide by the enzyme within the liposomes, i.e., internalization of the peptide. For the control experiment, LUVs in which the enzyme inhibitor was also encapsulated were used. The concentrations of trypsin and inhibitor inside the LUVs were 200 and 2000 μM, respectively.

Flip-Flop. The peptide-induced lipid flip-flop was detected as previously reported (*6*). NBD-labeled LUVs were generated from an equimolar mixture of EYPC and EYPG containing 0.5 mol % C_6-NBD-PC or C_{12}-NBD-PA. The symmetrically labeled vesicles were mixed with 1 M sodium dithionite/1 M Tris ([lipid] = 40 mM, [dithionite] = 60 mM) and incubated for 15 min at 30 °C to produce inner leaflet-labeled vesicles. The vesicles were immediately separated from dithionite by gel filtration (Bio-Gel A1.5m, 1.5 × 30 cm column). The fraction of NBD-lipids that had flopped during incubation in the absence or presence of the peptide was measured on the basis of fluorescence quenching by sodium dithionite. The asymmetrically NBD-labeled LUVs (2.0 mL) were incubated with or without the peptide for various periods at 30 °C. In the peptide-containing samples, 20 μL of a trypsin solution (5 mg/mL) was added to 2-mL samples and reacted for 1 min to hydrolyze the peptide. After addition of 20 μL of 1 M sodium dithionite/1 M Tris, NBD fluorescence was monitored with excitation and emission wavelengths of 460 and 530 nm, respectively. The percent flip-flop was calculated as described previously (*6*).

All the spectroscopic measurements described above were carried out at least in duplicate at 30 °C.

Antimicrobial Activity. The MICs of the peptides were determined as described by Park et al. (*25*). *Escherichia coli* cells (ATCC27325) were cultured in 3% (w/v) TSB at 37 °C overnight. To obtain mid-logarithmic phase microorganisms, 1 mL of the culture was then transferred to 100 mL of fresh TSB broth and incubated for 2−3 h. The cells were washed with cold 10 mM sodium phosphate buffer (pH 7.4) and resuspended in the same buffer. The cell concentrations were estimated by measuring absorbance at 600 nm on the basis of the predetermined relationship colony-forming units (cfu/mL = $ABS_{600}(3.8 \times 10^8)$. The suspension was diluted to 4×10^5 cfu/mL. The inoculum (90 μL) was added to each well of 96-well plates. The peptide samples (10 μL) were added to each well and incubated at 37 °C for 3 h. TSB [6% (w/v), 100 μL] was added (final cell concentration of 4×10^4 cfu/mL) and incubated at 37 °C for 12 h. Cell growth was assessed by measuring optical density of the culture at 620 nm on a Model 550 Microplate Reader (Bio-Rad, Hercules, CA). MIC was defined as the lowest concentration of peptide that inhibited growth.

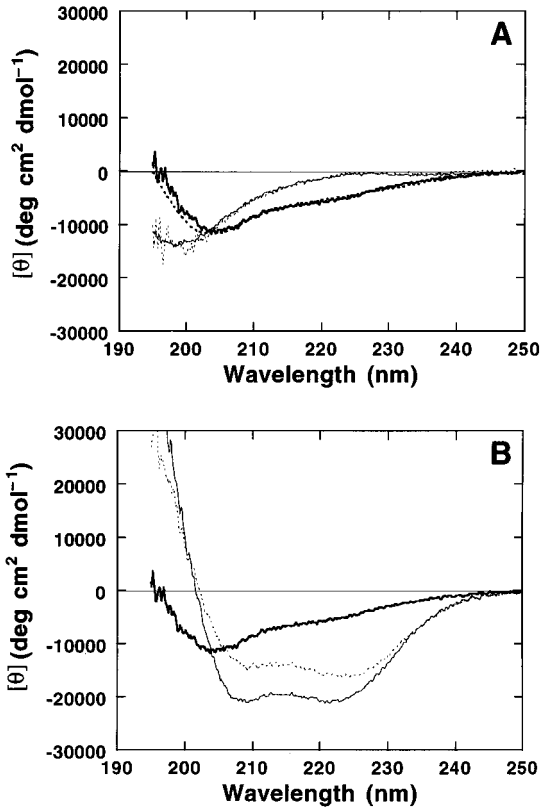

FIGURE 1: CD spectra. The CD spectra of BF2, MG2, and P11A-BF2 were measured at 30 °C ([peptide] = 25 μM). (A) Spectra of BF2 in phosphate buffer (10 mM sodium phosphate/45 mM NaCl/1 mM EDTA, pH 7.4), 1 mM EYPC SUVs, 1/1 (v/v) TFE/phosphate buffer (50 mM sodium phosphate, pH 7.0), and 1 mM EYPG SUVs are shown by dotted thin, solid thin, dotted thick, and solid thick curves, respectively. (B) Spectra of BF2, MG2, and P11A-BF2 in 1 mM EYPG SUVs are shown by solid thick, solid thin, and dotted thin curves, respectively.

Hemolytic Activity. Human erythrocytes (blood type O) from a healthy 22-year-old man were freshly prepared prior to the experiment. The blood was centrifuged (800*g*, 10 min) and washed 3 times with phosphate buffer (pH 7.4) to remove plasma and the buffy coat. Erythrocyte specimens were kept on ice throughout. Various concentrations of peptides were incubated with the erythrocyte suspension [final erythrocyte concentration 1% (v/v)] for 1 h at 37 °C. The percent hemolysis was determined from the optical density at 540 nm of the supernatant after centrifugation (800*g*, 10 min), as described elsewhere (*26*). Hypotonically lysed erythrocytes were used as the standard for 100% hemolysis.

RESULTS

CD. Figure 1A shows CD spectra of BF2 under various conditions. The peptide assumed an unordered structure in buffer. The presence of EYPC bilayers did not affect the spectrum, indicating that BF2 do not interact with the zwitterionic phospholipid. In contrast, BF2 bound to acidic EYPG bilayers, changing the secondary structure. However, the spectrum was different from that of MG2, which was a typical spectrum of an α-helix with double minima around 208 and 222 nm (Figure 1B). Rather, the spectrum of BF2 was superimposable on that in TFE/phosphate buffer (Figure 1A). The structure of BF2 in this mixed solvent was investigated previously by NMR (*27*). BF2 assumes a regular

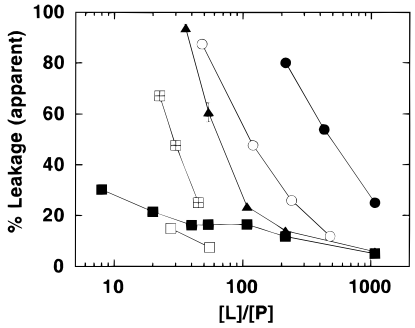

FIGURE 2: Estimation of membrane permeabilization activity. The peptides were added to ANTS/DPX-entrapping LUVs. The dye release was fluorometrically detected at 30 °C. The apparent percent leakage values for 10 min are plotted as a function of L/P. Peptides are symbolized as follows: circles, MG2; squares, BF2; triangles, P11A-BF2. Lipid compositions of LUVs are indicated as follows: closed symbols, EYPG/EYPC (1/1); open symbols, EYPG/EYPE (2/1); crossed squares, EYPG/EYPC (2/1).

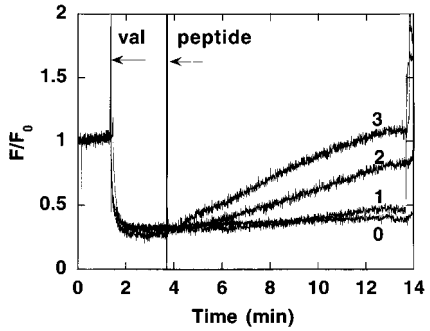

FIGURE 3: Detection of leakage of small ions. The peptides were added to K^+-loaded LUVs composed of EYPG/EYPC (1/1) suspended in isotonic K^+-free buffer, preequilibrated with the fluorescent dye $DiSC_2(5)$ and valinomycin. The dissipation of the diffusion potential by the leakage of small ions was monitored as the increase in fluorescence at 30 °C. Time courses of fluorescence change are shown by traces: trace 0, blank; trace 1, 1 μM BF2; trace 2, 1 μM P11A-BF2; trace 3, 0.5 μM MG2. [Lipid] = 215 μM.

helix in the C-terminal region, which is distorted around the Pro^{11} residue, whereas the N-terminal region is more flexible. BF2 is supposed to adopt a similar structure in EYPG membranes. Similarly to BF2, P11A-BF2 conformed to an unordered structure in buffer or in the presence of EYPC bilayers (data not shown). In the presence of EYPG, the peptide exhibited a CD spectrum similar to that of MG2 (Figure 1B). The spectrum of P11A-BF2 was not that of the completely membrane-bound form because further addition of EYPG SUVs resulted in deeper double minima. In contrast, the spectra of MG2 and BF2 in the presence of EYPG represented membrane-associated conformations because the CD spectra of both peptides showed no further changes when the concentration of EYPG SUVs was increased from 1 to 2 mM (data not shown).

Dye Leakage. Membrane permeabilization activity was estimated by the leakage of fluorescent dyes, ANTS/DPX, entrapped within LUVs. Figure 2 shows the apparent percent leakage value during a 10-min incubation as a function of L/P. BF2 (■) exhibited more than 100-fold weaker leakage activity compared with MG2 (●) against EYPG/EYPC (1/1) LUVs despite an order of magnitude higher antimicrobial activity. P11A-BF2 exhibited intermediate leakage activity (▲). The influence of the lipid composition was also investigated. An increase in EYPG content enhanced the leakage activity of BF2 (crossed squares), whereas the presence of EYPE lowered the activity (□). The dependence of BF2 leakage activity on lipid composition was similar to that of MG2 (○).

Diffusion Potential Assay. The diffusion potential assay can monitor the leakage of small ions from LUVs in the presence of a transmembrane potential. K^+-loaded EYPG/EYPC (1/1) vesicles were pretreated with the potential-sensitive fluorescent dye $DiSC_2(5)$ and valinomycin in K^+-free buffer. The dissipation of inside-negative diffusion potential after addition of peptide was detected as an increase in fluorescence (dequenching). Fluorescence intensity, F, was normalized to the initial fluorescence, F_0, after subtraction of the blank data without the dye. Trace 0 in Figure 3 shows the control experiment, where the buffer was added instead of the peptide. The addition of 0.5 μM MG2 caused significant dissipation of transmembrane potential (trace 3), whereas BF2 induced no measurable potential change even at 1 μM (trace 1). P11A-BF2 exhibited intermediate membrane-permeabilization activity (trace 2), as observed in the ANTS/DPX leakage experiments. It should be noted that the binding of the basic peptides may have caused expulsion of the positively charged dye $DiSC_2(5)$ from vesicles by electrostatic repulsion, preventing the dye from self-quenching. To investigate this effect, the same experiments were carried out in K^+ buffer, in which membrane potential was not generated by addition of valinomycin. We confirmed that the dye-releasing effect was negligible (data not shown). The addition of 0.2 μM MG2 showed little effect on membrane potential. The signal change was less than 10 percent of that at 0.5 μM (data not shown). Together with the results of dye leakage (Figure 2), these observations indicated that small ions cannot pass through the membrane at L/P ratios at which fluorescent dye leakage is not observed, excluding the possibility that a small pore or membrane lesion occurred before the formation of a larger supramolecular complex pore composed of aggregated helixes and lipids.

Peptide Translocation. Translocation of the peptides across lipid bilayers was detected as reported elsewhere (*7*). Trypsin was encapsulated within the internal aqueous phase of EYPC/EYPG/DNS-PE (50/45/5) LUVs to selectively digest the translocated peptide. The enzyme outside the vesicles was inactivated by trypsin−chymotrypsin inhibitor. The enzyme hydrolyzes the peptide bonds on the C-terminal sides of the Lys and Arg residues. The hydrolyzed Trp-containing fragments will be desorbed from the membrane and can be detected by the RET technique; desorption results in relief of RET, i.e., a decrease in dansyl fluorescence at 510 nm when excited at 280 nm, where Trp is selectively excited. As shown in Figure 4, BF2 (trace 4) was translocated across the membrane much more effectively than MG2 (trace 3). The translocation activity of P11A-BF2 was much closer to that of BF2 (trace 2). Trace 1 indicates the control experiment in which the enzyme inhibitor was also present inside the vesicles. No digestion was observed. The initial fluorescence value for MG2 was already saturated at L/P = 40 and scarcely changed when the L/P value was increased to 215. In contrast, the value for BF2 was increased by about 1.3-fold, reaching the same value as that of MG2. These observations indicated that MG2 has stronger binding affinity

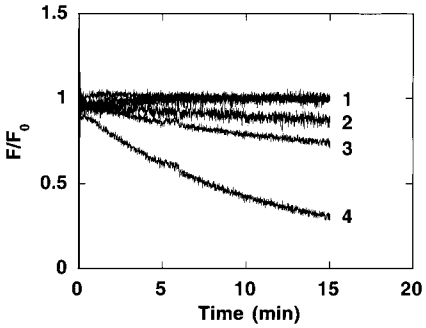

FIGURE 4: Detection of peptide translocation. The peptides were added to trypsin-entrapping LUVs (EYPC/EYPG/DNS-PE = 50/45/5) and the sensitized dansyl fluorescence at 510 nm was recorded on excitation of Trp residues at 280 nm. Decreases in fluorescence implied digestion of the fluorescent peptide by the enzyme within the liposomes, i.e., internalization of the peptide. The peptide concentration was 1 μM. Trace 2, P11A-BF2; trace 3, MG2; trace 4, BF2. Trace 1 shows the control experiment in which the enzyme inhibitor was also present in the LUVs. The lipid concentration was 215 μM. The data are expressed as F/F_0, where F_0 is the initial fluorescence value.

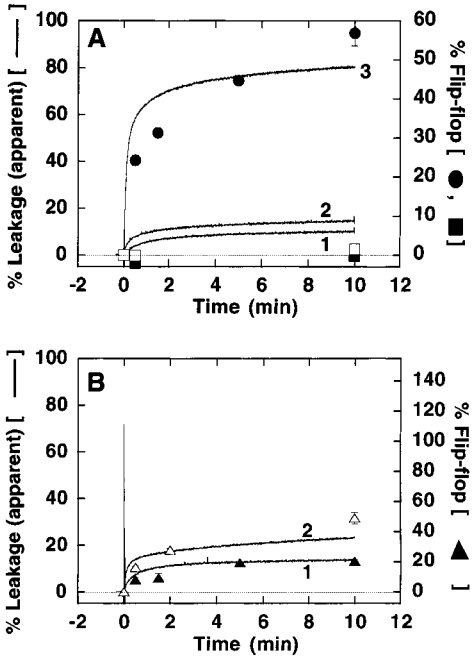

FIGURE 5: Coupling between dye leakage and lipid flip-flop. Time courses of ANTS/DPX apparent percent leakage and lipid flip-flop are shown by traces and symbols, respectively: (A) Trace 1 and ■, 1 μM BF2; trace 2 and □, 2 μM BF2; trace 3 and ●, 1 μM MG2. (B) Trace 1 and ▲, 1 μM P11A-BF2; trace 2 and △, 2 μM P11A-BF2. The lipid composition was EYPG/EYPC (1/1). For lipid flip-flop measurements, 0.5 mol % C_6-NBD-PC was included. [Lipid] = 215 μM.

for the negatively charged LUVs than BF2 and that both peptides are completely membrane-bound at L/P = 215.

Lipid Flip-Flop. MG2 induced the transbilayer movement of the fluorescent lipid C_6-NBD-PC (●) coupled with pore formation (trace 3) at a peptide concentration of 1 μM (Figure 5A). In contrast, BF2 triggered no measurable lipid flip-flop even at a higher peptide concentration of 2 μM (□), although the dye leakage was slightly increased (trace 2). As shown in Figure 5B, P11A-BF2 induced lipid flip-flop coupled with dye leakage in a dose-dependent manner. We also investigated the flip-flop of the acidic lipid C_{12}-NBD-PA (data not shown). MG2 (1 μM) induced almost the same extent of flip-flop as C_6-NBD-PC at 10 min. BF2 caused practically no lipid flip-flop at 1 μM and less than 10% flip-flop even at 2 μM. The flip-flop rate of C_{12}-NBD-PA was increased for P11A-BF2 at 1 μM compared with C_6-NBD-PC and showed almost the same rate as that of MG2.

Table 2: Antimicrobial and Hemolytic Activities

	MIC[a] (μM)	hemolysis (%)	[peptide][b] (μM)
MG2	24	7.7	694
BF2	3.2	2.5	810
P11A-BF2	6	7.3	806

[a] Minimal inhibitory concentration (MIC) against *E. coli* ATCC27325. [b] The peptide concentration at which hemolytic activity was measured.

Antimicrobial and Hemolytic Activity. Table 2 shows the antimicrobial activities of the three peptides against *E. coli* ATCC27325. BF2 exhibited a significantly higher antibacterial activity than MG2, as reported by Park et al. (*12*). P11A-BF2 showed a slightly less potent activity compared with BF2. The three peptides were practically nonhemolytic at concentrations more than 25-fold higher than the MICs. BF2 showed the highest selective toxicity and was nonhemolytic even at a concentration >200× MIC.

DISCUSSION

Selective Toxicity. Self-defense peptides should selectively kill bacteria without exerting significant toxicity against the host cells. BF2 as well as MG2 exhibit potent antimicrobial activities, whereas the peptides are practically nonhemolytic (Table 2). Negatively charged components on the bacterial cell surface such as acidic phospholipids, lipopolysaccharides, and teicoic acids have been suggested to constitute the chemoreceptors of positively charged peptides (*3*, *26*). Indeed, BF2 specifically binds to negatively charged EYPG (Figure 1A), as observed for MG2 (*26*, *28*) and PGLa (*11*). The affinity of BF2 for EYPC was less than that of MG2 because in the presence of 1 mM EYPC no change in CD spectrum was observed for BF2 (Figure 1A), whereas a significant change ($[\theta]_{222}$ from −1600 to −5200 deg cm^2 dmol^{-1}) was detected for MG2 (spectrum not shown). Hydrophobic interactions play a major role in binding to EYPC. The mean hydrophobicity of BF2 was appreciably smaller than that of MG2 (Table 1), in keeping with the binding data. The surface of erythrocyte membranes is exclusively composed of zwitterionic phospholipids, mainly phosphatidylcholine and sphingomyelin. BF2 was again less hemolytic than MG2 (Table 2).

Ultimate Target. The mechanism of antimicrobial activity of MG2 is considered to be the permeabilization of cell membranes. Addition of the peptide to *E. coli* cells leads to cell death concomitant with intracellular K^+ leakage (*29*) and cell lysis (*13*) within a few minutes. MG2 also destroyed the barrier property of artificial lipid bilayers (Figures 2 and 3; see also refs *5*, *9*, *11*, *26*, *28*, and *30*). In contrast, despite its stronger antimicrobial activity, BF2 did not induce appreciable membrane permeabilization (Figure 2) even in the presence of trans-negative potential (Figure 3) under comparable conditions. Instead, BF2 was translocated into the vesicle interior more efficiently than MG2 (Figure 4). These observations suggested that the ultimate targets of BF2 are intracellular components rather than cell membranes. As a measure of intracellular preference or translocation ef-

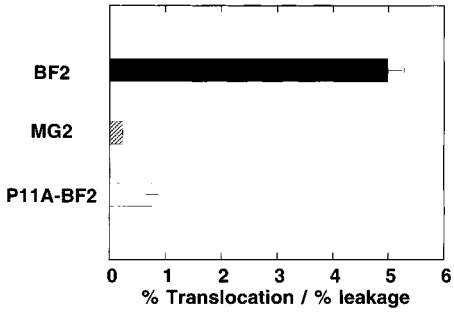

FIGURE 6: Translocation efficiency. Translocation efficiency was defined as % translocation/% leakage for 10 min obtained from Figures 4 and 5. [Peptide] = 1 μM, [lipid] = 215 μM.

ficiency, the percent translocation/percent leakage values under the same conditions are compared in Figure 6. The translocation efficiency of BF2 was ~20-fold greater than that of MG2. Indeed, BF2 has been shown to enter *E. coli.* cells, killing the bacteria without cell lysis (*13*). BF2 exhibits 20-fold higher affinity for nucleic acids than MG2 (*13*). Therefore, BF2 appears to inhibit cellular functions by binding to DNA and/or RNA.

Translocation Mechanism. MG2 forms a dynamic, peptide−lipid supramolecular complex pore, inducing mutually coupled dye leakage and flip-flop (*3*, *4*, *6*; see also Figure 5A). Formation of the "toroidal pore" (*31*) requires the induction of positive (convex) curvature in lipid bilayers in the direction along the helix axis (*30*). In fact, MG2 raises T_H of DPoPE, suggesting that the peptide inhibits the formation of inverted structures by imposing positive curvature strain (*30*). In accordance with this view, the presence of negative curvature-inducing EYPE inhibits pore formation (Figure 2).

In contrast to MG2, BF2 is efficiently translocated across lipid bilayers without significant membrane permeabilization or lipid flip-flop (Figure 5A). If the peptide permeates membranes via pore formation, the observed effective translocation should be the consequence of fast formation and disintegration of the pore because translocation occurs upon pore disintegration. BF2 also appears to impose positive curvature strain in lipid bilayers; the presence of EYPE inhibits BF2-induced dye leakage at higher peptide concentrations (Figure 2). Formation of a toroidal pore demands negative curvature in the direction perpendicular to the surface-lying helix axis in the plane of the bilayer (*3*, *30*). Therefore, peptides with narrower angles subtended by the polar face of an amphipathic helix show faster pore formation (*11*, *32*, *33*). The polar face angle of BF2 helix was about 180° (*27*), which is close to that of the MG2 helix. Thus, the polar angle does not contribute to fast pore formation. A large positive charge of BF2 (+6) results in pore destabilization because of enhanced electrostatic repulsion. However, this alone cannot explain the absence of membrane permeabilization because amphiphilic peptides with a charge of +6 such as P11A-BF2 (Figure 2) and model peptides (*32*) generally show measurable dye leakage as well as lipid flip-flop under the conditions in which translocation occurs.

Role of Pro. Pro → Ala substitution caused BF2 to show magainin-like properties in terms of conformation (Figure 1B), translocation efficiency (Figure 6), and leakage-coupled lipid flip-flop (Figure 5B). BF2 conforms to a bent helix with the flexible N-terminal region in TFE/buffer and probably in EYPG bilayers (Figure 1A). The unusual helical conformation of the Pro^{11}-containing segment (Ala^6−Val^{12}) extends the otherwise limited amphipathic region (Pro^{11}−Lys^{21}) to the residues involving Ala^6 through Lys^{21} (*27*). Dempsey's group (*34*) suggested that the G-X-X-P motif found in alamethicin is responsible for the backbone flexibility of the peptide. In the case of BF2, the G^7-X-X-X-P^{11} segment may provide flexibility related to efficient translocation via an unknown mechanism because of the distorted helical conformation with a larger diameter and greater pitch (*27*). Substitution of Ala for Pro is known to *destabilize* the ion channels of alamethicin (*35*, *36*) and trichosporin B VIa (*37*), as well as melittin (*38*). If this also occurred for a putative BF2 pore, it would facilitate peptide translocation contrary to the observed inhibition of translocation.

In summary, it is highly likely that BF2 has a novel translocation mechanism other than that mediated via formation of peptide−lipid supramolecular pores, although the presence of an extremely unstable pore cannot be excluded. We are currently investigating the translocation mechanism of BF2 in more detail.

REFERENCES

1. Hancock, R. E. W., and Lehrer, R. (1998) *Trends Biotechnol. 16*, 82−88.
2. Zasloff, M. (1987) *Proc. Natl. Acad. Sci. U.S.A. 84*, 5449−5453.
3. Matsuzaki, K. (1999) *Biochim. Biophys. Acta 1462*, 1−10.
4. Matsuzaki, K. (1998) *Biochim. Biophys. Acta 1376*, 391−400.
5. Matsuzaki, K., Murase, O., Tokuda, H., Funakoshi, S., Fujii, N., and Miyajima, K. (1994) *Biochemistry 33*, 3342−3349.
6. Matsuzaki, K., Murase, O., Fujii, N., and Miyajima, K. (1996) *Biochemistry 35*, 11361−11368.
7. Matsuzaki, K., Murase, O., Fujii, N., and Miyajima, K. (1995) *Biochemistry 34*, 6521−6526.
8. Matsuzaki, K., Murase, O., and Miyajima, K. (1995) *Biochemistry 34*, 12553−12559.
9. Matsuzaki, K., Nakamura, A., Murase, O., Sugishita, K., Fujii, N., and Miyajima, K. (1997) *Biochemistry 36*, 2104−2111.
10. Matsuzaki, K., Yoneyama, S., Murase, O., and Miyajima, K. (1996) *Biochemistry 35*, 8450−8456.
11. Matsuzaki, K., Mitani, Y., Akada, K., Murase, O., Yoneyama, S., Zasloff, M., and Miyajima, K. (1998) *Biochemistry 37*, 15144−15153.
12. Park, C. B., Kim, M. S., and Kim, S. C. (1996) *Biochem. Biophys. Res. Commun. 218*, 408−413.
13. Park, C. B., Kim, H. S., and Kim, S. C. (1998) *Biochem. Biophys. Res. Commun. 244*, 253−257.
14. Kim, H. S., Park, C. B., Kim, M. S. N., and Kim, S. C. (1996) *Biochem. Biophys. Res. Commun. 229*, 381−387.
15. Chitnis, S. N., Prasad, K. S., and Bhargava, P. M. (1990) *J. Gen. Microbiol. 136*, 463−469.
16. Boman, H. G., Agerbath, B., and Boman, A. (1993) *Infect. Immun. 61*, 2978−2984.
17. Subbalakshmi, C., and Sitaram, N. (1998) *FEMS Microbiol. Lett. 160*, 91−96.
18. Wu, M., Maier, E., Benz, R., and Hancock, R. E. W. (1999) *Biochemistry 38*, 7235−7242.
19. Bartlett, G. R. (1959) *J. Biol. Chem. 234*, 466−468.
20. Takakuwa, T., Konno, T., and Meguro, H. (1985) *Anal. Sci. 1*, 215−218.
21. Matsuzaki, K., Nakai, S., Handa, T., Takaishi, Y., Fujita, T., and Miyajima, K. (1989) *Biochemistry 28*, 9392−9398.
22. Ladokhin, A. S., Wimley, W. C., and White, S. H. (1995) *Biophys. J. 69*, 1964−1971.
23. Shai, Y., Bach, D., and Yanovsky, A. (1990) *J. Biol. Chem. 265*, 20202−20209.
24. Oren, Z., Hong, J., and Shai, Y. (1997) *J. Biol. Chem. 272*, 14643−14649.

25. Park, I. Y., Park, C. B., Kim, M. S., and Kim, S. C. (1998) *FEBS Lett. 437*, 258−262.
26. Matsuzaki, K., Sugishita, K., Fujii, N., and Miyajima, K. (1995) *Biochemistry 34*, 3423−3429.
27. Yi, G. S., Park, C. B., Kim, S. C., and Cheong, C. (1996) *FEBS Lett. 398*, 87−90.
28. Matsuzaki, K., Harada, M., Funakoshi, S., Fujii, N., and Miyajima, K. (1991) *Biochim. Biophys. Acta 1063*, 162−170.
29. Matsuzaki, K., Sugishita, K., Harada, M., Fujii, N., and Miyajima, K. (1997) *Biochim. Biophys. Acta 1327*, 119−130.
30. Matsuzaki, K., Sugishita, K., Ishibe, N., Ueha, M., Nakata, S., Miyajima, K., and Epand, R. M. (1998) *Biochemistry 37*, 11856−11863.
31. Ludtke, S. J., He, K., Heller, W. T., Harroun, T. A., Yang, L., and Huang, H. W. (1996) *Biochemistry 35*, 13723−13728.
32. Matsuzaki, K., and Uematsu, N. (1999) *Biophys. J. 76*, A218.
33. Wieprecht, T., Dathe, M., Epand, R. M., Beyermann, M., Krause, E., Maloy, W. L., MacDonald, D. L., and Bienert, M. (1997) *Biochemistry 36*, 12869−12880.
34. Gibbs, N., Sessions, R. B., Williams, P. B., and Dempsey, C. E. (1997) *Biophys. J. 72*. 2490−2495.
35. Kaduk, C., Duclohier, H., Dathe, M., Wenschuh, H., Beyermann, M., Molle, G., and Bienert, M. (1997) *Biophys. J. 72*, 2151−2159.
36. Duclohier, H., Molle, G., Dugast, J. Y., and Spach, G. (1992) *Biophys. J. 63*, 868−873.
37. Nagaoka, Y., Iida, A., Kambara, T., Asami, K., Tachikawa, E., and Fujita, T. (1996) *Biochim. Biophys. Acta 1283*, 31−36.
38. Dempsey, C. E., Bazzo, R., Harvey, T. S., Syperek, I., Boheim, G., and Campbell, I. D. (1991) *FEBS Lett. 281*, 240−244.
39. Fauchère, J., and Pliška, V. (1983) *Eur. J. Med. Chem. 18*, 369−375.

BI0004549